

ing of perturbations. This could partly account for the more rapid convergence to bulk for Ni clusters than for Co and Fe clusters (15). Furthermore, we suspect that spin-wave structures are also responsible for the weak superimposed oscillations; however, our model is too crude to reveal these details.

The ferromagnetic state not only requires (quasilocal) magnetic moments but also requires that the moments remain mutually aligned even at relatively high temperatures (because of the strong interatomic exchange interaction, characteristic for ferromagnets) (1, 4). Temperature-dependent measurement of $\bar{\mu}$ in Fig. 3 show that this is indeed the case even for the smallest clusters. For example, the bulk $\bar{\mu}$ for Ni clusters is practically constant up to 300 K and decreases at higher temperatures, which indicates that for them the interaction affecting the mutual alignment is on the same order as in the bulk. Also the Ni₅₅₀₋₆₀₀ data are already quite bulklike, apart from the smoother transition near T_C . The latter is a characteristic small particle effect (19) [found qualitatively in Heisenberg model calculations (20) shown in Fig. 3]. Similar conclusions can be drawn for Co clusters; however, $\bar{\mu}$ increases slightly with increasing T . This could be related to a smaller ($\approx 1.5\%$) increase observed in the bulk at 650 K where it is caused by the phase transition from hexagonal close-packed to face-centered-cubic (21).

Compared with Ni and Co clusters, Fe clusters are clearly anomalous. Anomalies in Fe clusters may be expected because, for Fe, in contrast with Ni and Co, the magnetic moment is very sensitive to its environment: changes in the crystal structure strongly affect the magnetic moment (1, 17). For Fe₁₂₀₋₁₄₀ near 600 K, one observes a rather pronounced decrease in $\bar{\mu}$ from about $3\mu_B$ to about $0.6\mu_B$. Larger clusters have high-temperature moments of about $0.4\mu_B$. These effects most likely reflect related behavior in the bulk where the low-temperature, body-centered-cubic phase with $\bar{\mu} = 2.2\mu_B$ transforms into a low moment face-centered-cubic phase at $T = 1150$ K (that is, above $T_C = 1043$ K) (8). Apparently, in Fe clusters this phase transition occurs at progressively lower temperatures as the cluster size is increased. Clearly this trend must reverse for sizes larger than measured here to correspond with the bulk.

In conclusion, our molecular beam measurements on ferromagnetic clusters show the evolution of ferromagnetism from the atom to the bulk. The development occurs gradually and appears to be dominated primarily by electronic effects caused by the surface, which affect the magnetic moments of atoms rather deep inside the clusters. The Heisenberg model calculations poorly re-

produce the experimental data in Fig. 3A, because in those calculations only nearest neighbor interactions are taken into account and the local magnetic moments are independent of their location in the cluster. For Ni and Co clusters we essentially traced the evolution from atom to the bulk. However, the transition temperature to the low moment phase of Fe clusters continues to decrease. Further study is required to better understand this transition and how it converges to its bulk limit.

REFERENCES AND NOTES

1. D. C. Mattis, *The Theory of Magnetism* (Springer-Verlag, Berlin, ed. 2, 1988); C. Herring, in *Magnetism*, vol. 4, G. T. Rado and H. Suhl, Eds. (Academic Press, New York, 1966).
2. J. Dorantes-Davila, H. Dreyssé, G. Pastor, *Phys. Rev. B* **46**, 10432 (1992); M. R. Press, F. Liu, S. N. Khanna, P. Jena, *ibid.* **40**, 399 (1989); C. Y. Yang, K. H. Johnson, D. R. Salahub, J. Kasper, R. P. Messmer, *ibid.* **24**, 5673 (1981); K. Lee, K. Callaway, K. Kwong, R. Tang, A. Ziegler, *ibid.* **31**, 1796 (1985).
3. A. J. Freeman, C. Li, R. Q. Wu, in *Science and Technology of Nanostructured Magnetic Materials*, G. C. Hadjipanayis and G. A. Prinz, Eds. (NATO Advanced Study Institutes, Series B, vol. 259, Plenum, New York, 1991), pp. 1-13.
4. N. W. Ashcroft and N. D. Mermin, *Solid State Physics* (Holt, Rinehart & Winston, New York, 1976); C. Kittel, *Introduction to Solid State Physics* (Wiley, New York, 1976).
5. K. Haneda, Z. X. Zhou, A. H. Morrish, T. Majima, T. Miyahara, *Phys. Rev. B* **46**, 13832 (1992), and references therein.
6. For a review of cluster beam methods, see W. A. de Heer, *Rev. Mod. Phys.* **65**, 611 (1993).
7. D. A. Papaconstantanopoulos, in *Handbook of the Band Structure of Elemental Solids* (Plenum, New York, 1986), p. 73.
8. M. B. Stearns, in *Magnetische Eigenschaften von Metallen*, Landolt and Börnstein, Eds. (Springer-Verlag, Berlin, 1986), New Series III/19a, p. 24.
9. A. J. Freeman, C. L. Fu, S. Ohnishi, M. Weinert, in *Polarized Electrons in Surface Physics*, R. Feder, Ed. (World Scientific, Singapore, 1985), pp. 3-66.
10. M. B. Stearns, *Phys. Rev. B* **4**, 4081 (1971), and references therein.
11. W. A. de Heer, P. Milani, A. Chatelain, *Phys. Rev. Lett.* **65**, 488 (1990); J. P. Bucher, D. C. Douglass, L. A. Bloomfield, *ibid.* **66**, 3052 (1991).
12. I. M. L. Billas, J. A. Becker, A. Chatelain, W. A. de Heer, *ibid.* **71**, 4067 (1993).
13. P. Milani and W. A. de Heer, *Rev. Sci. Instrum.* **61**, 1835 (1990); W. A. de Heer and P. Milani, *ibid.* **62**, 670 (1991).
14. V. A. Gubanov, A. I. Liechenstein, A. V. Postnikov, *Magnetism and Electronic Structure of Crystals* (Springer-Verlag, Berlin, 1992), p. 79.
15. O. Erikson, A. M. Boring, R. C. Albers, G. W. Fernando, B. R. Cooper, *Phys. Rev. B* **45**, 2868 (1992), and references therein.
16. E. Wimmer, A. J. Freeman, K. Krakauer, *ibid.* **30**, 3113 (1984).
17. R. Wu and A. J. Freeman, *ibid.* **47**, 3904 (1993), and references therein.
18. C. S. Wang and A. J. Freeman, *ibid.* **24**, 4364 (1981).
19. Y. Imry, *ibid.* **21**, 2042 (1980); M. E. Fisher and A. N. Berker, *ibid.* **26**, 2507 (1982).
20. K. Binder, H. Rauch, V. Wildpaner, *J. Phys. Chem. Solids* **31**, 391 (1990).
21. E. P. Wohlfarth, in *Ferromagnetic Materials*, E. P. Wohlfarth, Ed. (North-Holland, New York, 1980), vol. 1, pp. 3-70; H. P. Myers and W. Sucksmith, *Proc. R. Soc. London Ser. A* **207**, 427 (1951); M. Pellarin et al., *Chem. Phys. Lett.* **217**, 349 (1994).
22. We thank P. Ballone for continued interest and valuable suggestions. This research is supported by the Swiss National Fund.

19 May 1994; accepted 26 July 1994

All-Polymer Field-Effect Transistor Realized by Printing Techniques

Francis Garnier,* Ryad Hajlaoui, Abderrahim Yassar, Pratima Srivastava

A field-effect transistor has been fabricated from polymer materials by printing techniques. The device characteristics, which show high current output, are insensitive to mechanical treatments such as bending or twisting. This all-organic flexible device, realized with mild techniques, opens the way for large-area, low-cost plastic electronics.

Organic semiconducting materials, such as conjugated polymers and oligomers, have recently been used as active layers in electronic devices, such as field-effect transistors (FETs) (1) and electroluminescent diodes (LEDs) (2). By a further use of organic compounds as substrates or contact electrodes, "all-organic" devices were developed first for FETs (3) and later for LEDs (4), thereby creating the promising perspective of low-cost and large-area fabrication of flexible devices. However, the term all-or-

ganic is in its strictest sense misleading because the reported structures still contain a metallic part, the gold source and drain electrodes in FETs or the rectifying calcium or magnesium electrode in LEDs. The deposition process of these electrodes, requiring high vacuum and temperature, creates a constraining costly step in the device fabrication. Furthermore, these metal-organic interfaces, which cannot be considered as fully flexible, form a potential source of mechanical and chemical instability. We report here a fully organic device, an all-polymer FET fabricated solely by printing techniques, which opens the field of flexible plastics electronics.

Laboratoire des Matériaux Moléculaires, CNRS, 2 rue Dunant, 94320 Thiais, France.

*To whom correspondence should be addressed.

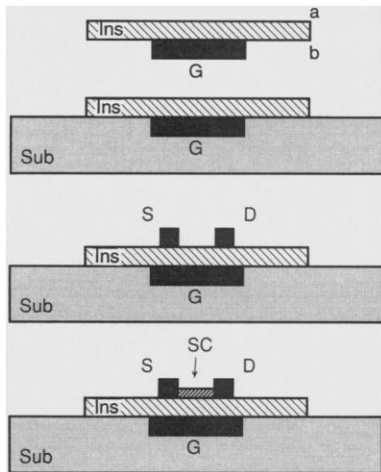


Fig. 1. Steps for the construction of an all-polymer FET: cross section of the insulating layer (Ins), the gate electrode (G), the substrate (Sub), the source and drain electrodes (S and D, respectively), and the organic semiconductor (SC).

The easiest route for device fabrication (Fig. 1) is to start from the insulating layer. As often pointed out in device technology, one of the critical components of metal-insulator-semiconductor FETs is the thin insulating layer, which must show high homogeneity and good dielectric properties (5). These characteristics can be obtained easily from commercially available materials, such as the 1.5- μm -thick polyester film polyethylene terephthalate (Goodfellow, Cambridge, United Kingdom), which presents a high resistivity, $\rho > 10^{14} \Omega \text{ cm}$, and has a dielectric constant, ϵ , of 3.0. A $10 \times 15 \text{ mm}$ sized polyester film was fixed to a frame to ensure flatness of the film. The first step concerned the gate electrode (G), which was made by depositing, through a $5 \times 12 \text{ mm}$ mask on one of the faces (b) of the insulating film (Ins) a 10- μm -thick layer of a conducting graphite-based polymer ink (Electrodag 423, Acheson Colloiden B. V., Scheemda, Netherlands). The device substrate (Sub), providing flexible mechanical support and self-standing properties to the device, was applied in step 2 to the b face of insulating film. It consists of a $10 \times 15 \text{ mm}$ sized adhesive tape with electrical contact for the gate electrode made from the same conducting polymer ink. The third step involved the deposition of the source and gate electrodes on the opposite face, a, of the insulating film. Two $1 \times 10 \text{ mm}$ strips 10 μm thick of the same conducting graphite-based polymer ink, forming the source (S) and drain (D) electrodes, were deposited through a mask with a 200- μm inter-electrode distance, corresponding to channel width (W) and length (L) of 10 mm and 200 μm , respectively. The device was then completed by depositing the organic

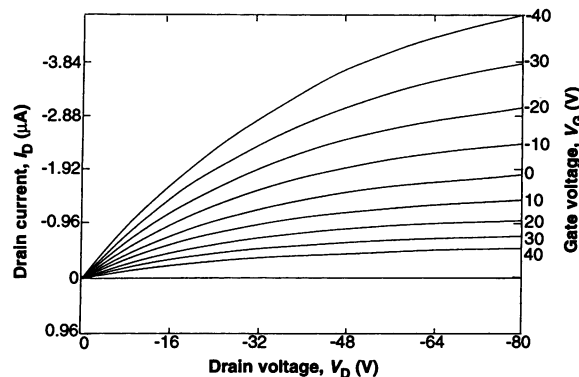


Fig. 2. Uncorrected drain current (I_D) versus drain voltage (V_D) curves for various gate voltages (V_G) measured on an all-polymer FET with a polyester insulating layer ($C_i = 1.5 \text{ nF cm}^{-2}$) and a 40-nm-thick α, ω -di(hexyl)sexithiophene semiconducting layer. Gate source and drain electrodes are made from a conducting graphite-based polymer ink.

semiconducting layer, SC, for which α, ω -di(hexyl)sexithiophene was chosen, owing to its high field-effect mobility ($\mu_{\text{FET}} = 7 \times 10^{-2} \text{ cm}^2 \text{ V}^{-1} \text{ s}^{-1}$). The field-effect mobility has been interpreted on the basis of the highly ordered structure resulting from self-assembly properties of this semiconductor (6). The semiconductor layer was realized by a flash evaporation at 350°C of a small amount of the semiconductor in a crucible. The simultaneous deposition of the semiconductor on a reference glass side allowed us to determine, from its absorption spectrum, the thickness of the semiconductor layer of about 40 nm. The realized FET therefore corresponds to a true all-polymer device, fabricated only by the use of printing techniques.

The electrical characteristics of this device have been measured in air, at room temperature, and in a metal box that provides electrical shielding. Current voltage characteristics were obtained with a Hewlett-Packard (HP) 4140 B picoameter/dc voltage source, and capacitance was obtained with an HP 4192A impedance analyzer. The ohmic resistance of the source and drain electrodes, on the order of 10^3 ohms, is low enough for the current intensities expected for this device. The measured capacitance of the polyester layer, $1.5 \times 10^{-9} \text{ F cm}^{-2}$, agrees with the value calculated from the insulator film thickness and dielectric constant.

The uncorrected current-voltage (I_D - V_D) curves at constant gate bias V_G (Fig. 2) show that excellent amplification characteristics are obtained with this all-polymer FET device with currents in the microampere range. Depletion and accumulation regimes are clearly observed under positive and negative gate bias, demonstrating the *p*-type character of this semiconductor, as previously observed with FET devices based on these organic semiconductors but with metallic electrodes (1, 6). The absence of leakage current confirms the good properties of the insulating layer. Furthermore, the absence of significant hysteresis in the drain current-gate voltage (I_D - V_G) curves, at constant drain voltage (Fig. 3), rules out the

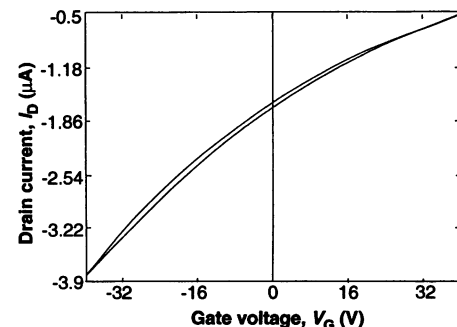


Fig. 3. Drain current versus gate voltage at a constant drain voltage of -40 V for an all-polymer FET (same characteristics as in Fig. 2).

contribution of charging effects in the dielectric layer. The field-effect mobility was calculated from the transconductance (g_m) in the linear regime (5, pp. 200–216) from

$$g_m = (\delta I_D / \delta V_G)_{V_D = \text{cst}} = (W/L) C_i \mu_{\text{FET}} V_D \quad (1)$$

where I_D is the drain current, V_G and V_D are the gate and drain voltages, respectively, C_i is the capacitance, and *cst* is a constant. The value for μ_{FET} of $6 \times 10^{-2} \text{ cm}^2 \text{ V}^{-1} \text{ s}^{-1}$ is in excellent agreement with that obtained for devices fabricated by classical technology (6) and close to that of amorphous hydrogenated silicon conventionally used in FETs (between 10^{-1} and $1 \text{ cm}^2 \text{ V}^{-1} \text{ s}^{-1}$) (7). A series of mechanical operations on this device such as rolling-up, bending, and twisting at 90° did not affect the electrical characteristics, whereas similar operations performed on a previously reported organic FET with metallic electrodes (3) led to disconnecting. This result emphasizes the flexibility reached by the present all-polymer device.

The characteristics of these devices are governed by many parameters. Lowering the insulating film thickness and increasing its dielectric constant (by the use of, for instance, polyimide) should increase the capacitance of the device and so improve its response. On the other hand, the intrinsic carrier mobility of thiophene

oligomers can still be increased by a structural control of molecular organization, as shown in recent work (8). The solubility of these oligomers in chlorinated solvents, such as dichloromethane or 1,1,2,2-tetrachloroethane, is high enough to produce thin films by spin-coating or casting techniques (9), which widens the technological access to such all-polymer devices. Any kind of substrate can be considered in step 2, depending on the mechanical properties desired for the device. Concerning the gate, source, and drain electrodes, a silver paste-based polymer ink (Acheson) has also been successfully used in this work. However, other organic-based materials could be used, such as conducting polyaniline polypyrrole or polythiophenes (10–12), with achievable resolution as the goal. Although the present device is largely oversized, conventional printing techniques would allow us to reach some 50 μm for channel length, which means that channel widths of 0.5 to 1 mm would be required to effect significant amplification. These dimensions may appear large, but recent reports have pointed out that an interesting potential exists for macrosized chips in the display area (13). It must also be stressed that patterning techniques applied to organic conducting polymers have been shown to allow the realization of micrometer-sized electrode arrays, which should extend the possibilities of such all-polymer devices to a readily usable device (10). This work has shown that devices fully based on polymer materials can be fabricated by only the use of printing techniques, and the interesting results appear promising for the development of large-area, low-cost plastic electronics.

REFERENCES AND NOTES

1. G. Horowitz, D. Fichou, X. Z. Peng, Z. G. Xu, F. Garnier, *Solid State Commun.* **72**, 381 (1989).
2. J. H. Burroughes *et al.*, *Nature* **347**, 539 (1990).
3. F. Garnier, X. Z. Peng, G. Horowitz, D. Fichou, *Adv. Mater.* **2**, 592 (1990).
4. G. Gustafsson *et al.*, *Nature* **357**, 477 (1992).
5. S. M. Sze, *Semiconductor Devices, Physics and Technology* (Wiley, New York, 1985), pp. 341–362.
6. F. Garnier *et al.*, *J. Am. Chem. Soc.* **115**, 8716 (1993).
7. G. W. Neudeck and A. K. Malhotra, *Solid State Electron.* **19**, 721 (1976).
8. B. Servet *et al.*, *Chem. Mater.*, in press.
9. S. Hotta and K. Waragai, *Adv. Mater.* **5**, 896 (1993).
10. M. Angelopoulos *et al.*, *Polym. Eng. Sci.* **32**, 1535 (1992).
11. O. Inganäs, G. Gustafsson, C. Svensson, *Synth. Met.* **41–43**, 1095 (1991).
12. H. Naarmann, in *Science and Applications of Conducting Polymers*, W. R. Salaneck, D. T. Clark, E. J. Samuelsen, Eds. (Hilger, New York, 1990), p. 81.
13. R. A. Street, *Mater. Res. Soc. Bull.* **17**, 70 (1992).
14. We thank G. Horowitz for helpful discussions, the Conseil Général du Val de Marne for financial support, and M.C.G. for personal contribution to this work.

6 June 1994; accepted 16 July 1994

The Unidentified Interstellar Infrared Bands: PAHs as Carriers?

S. Schlemmer, D. J. Cook, J. A. Harrison, B. Wurfel, W. Chapman, R. J. Saykally*

Infrared emission spectra of gas-phase naphthalene and pyrene have been measured in the range of 3 to 7.5 micrometers with ultraviolet laser desorption-excitation and a spectroscopic technique featuring single-photon counting in the infrared. The spectra were compared with the unidentified infrared emission bands that are observed in many astronomical objects. Marked discrepancies between those observations and the laboratory emission spectra in the wavelengths and relative intensities of principal spectral features led to the conclusion that small neutral unsubstituted polycyclic aromatic hydrocarbons cannot be the carriers of the unidentified infrared emission bands.

One of the most intriguing current problems in astrophysics is to identify the carriers of the visible diffuse interstellar absorption bands (DIBs) (1) and the unidentified infrared emission bands (UIRs) (2). These emission bands are observed from a variety of astronomical objects, including planetary nebulae (3), reflection nebulae (4, 5), HII regions (6), and galactic nuclei (7), all of which exhibit the same principal spectral features, which seem to correlate with the abundance of carbon (5). The identification of the carriers is important because they could account for a significant fraction of carbon in the interstellar medium. The hypothesis that the carriers of the UIRs are polycyclic aromatic hydrocarbon (PAH) molecules (8) has received much attention, supported by the identification of these species in interplanetary dust particles (9). According to the PAH hypothesis (2), individual PAHs absorb ultraviolet (UV) radiation emitted from nearby hot stars, undergo internal conversion or intersystem crossing followed by internal vibrational redistribution on a time scale shorter than UV fluorescence, and finally, emit infrared (IR) radiation characteristic of the aromatic C–H stretch [3.3 μm , (3040 cm^{-1})], C–C stretch [6.2 μm (1615 cm^{-1}) and 7.7 μm (1310 cm^{-1})], C–H in-plane bend [8.6 μm (1160 cm^{-1})], and C–H out-of-plane bend [11.3 μm (885 cm^{-1}) and 12.7 μm (785 cm^{-1})]. These six features correspond to the major UIRs.

The similarity of the observed UIRs to the absorption spectra of several PAH molecules has been described (2). However, emission and absorption spectra can differ markedly, especially if the vibrational energy content of the molecule is high and many overtones and combination bands are excited. Therefore, only laboratory emission experiments can test the PAH hypothesis

in a rigorous way. Previous emission measurements were confined to the 3- to 4- μm wavelength range, characteristic of aromatic and aliphatic C–H stretch vibrations (10–14). The 3.3- μm features observed in previous experiments were found to coincide with essentially all astronomical UIR observations. Moreover, the emission spectra observed for different PAHs excited by different UV wavelengths are strikingly similar. Thus, the general notion that PAHs are responsible for the interstellar IR emission features seems supported by the available evidence. However, the 3.3- μm C–H stretch is ubiquitous to a wide variety of hydrocarbons; an identification of the UIR carriers from observation of the 3.3- μm emission alone is impossible.

In this report we describe the measurement of IR emission spectra for two representative small neutral PAHs—naphthalene and pyrene—in the extended range of 3 to 7.5 μm with the use of an infrared photon counting technique that we have developed. In these experiments we simultaneously monitor several of the principal UIR features, which allows us to assess the identification of their carriers in a more definitive manner than has been possible before.

Previous laboratory emission experiments addressing the PAH hypothesis have involved a direct simulation of the proposed mechanism with UV excitation of small PAH molecules under collision-free conditions (10, 11, 13). PAHs larger than benzene or naphthalene have vapor pressures suitable for spectroscopy only at high temperatures. Thermal sources of gaseous PAHs therefore emit intense blackbody radiation, which limits the sensitivity of conventional IR emission experiments and renders measurements beyond 4 μm extremely difficult.

Our experimental approach is to use UV-laser-induced desorption (UV-LID) to vaporize PAH molecules adsorbed on a 77-K sample plate. The 248-nm excimer laser light also provides the requisite elec-

Department of Chemistry, University of California, Berkeley, CA 94720–1460, USA.

*To whom correspondence should be addressed.